Chapter 1

Introduction

1.1 Introduction of Liquid Crystal

Liquid crystalline phase is first discovered by Dr. F. Reinizer [1] in 1888 and the well known term “liquid crystal” is introduced by Lehmann [2] in 1890. Liquid crystals are substances that exhibit a phase of matter that has properties between those of an isotropic liquid, and those of a solid crystal. Common materials that are liquid crystals include cholesteryl esters, lectithin, DNA, cellulose, and graphite. There are many different types of liquid crystal phases, also called “mesophases”, which can be distinguished based on their different optical properties. Because a liquid crystal have the property that scatters light that shines on it, liquid crystals are often used to display letters and numbers on calculators and digital watches or to test for heat-sensitive areas on other materials. Liquid-crystal systems exist for hand-held television sets and large, flat projection screens for TV have now been developed, as have liquid-crystal computer displays.

1.2 Liquid Crystal Phase

Liquid crystal phases are classified by several configurations of molecules which widely differ in their structure. Generally, rod-like molecules tend to orient themselves around the rubbing direction and align parallel to each other to a preferred direction which is so called self-assembly. The three major types of liquid crystals—nematic, smectic, and

cholesteric —are designated by the amount of the order in the materials.

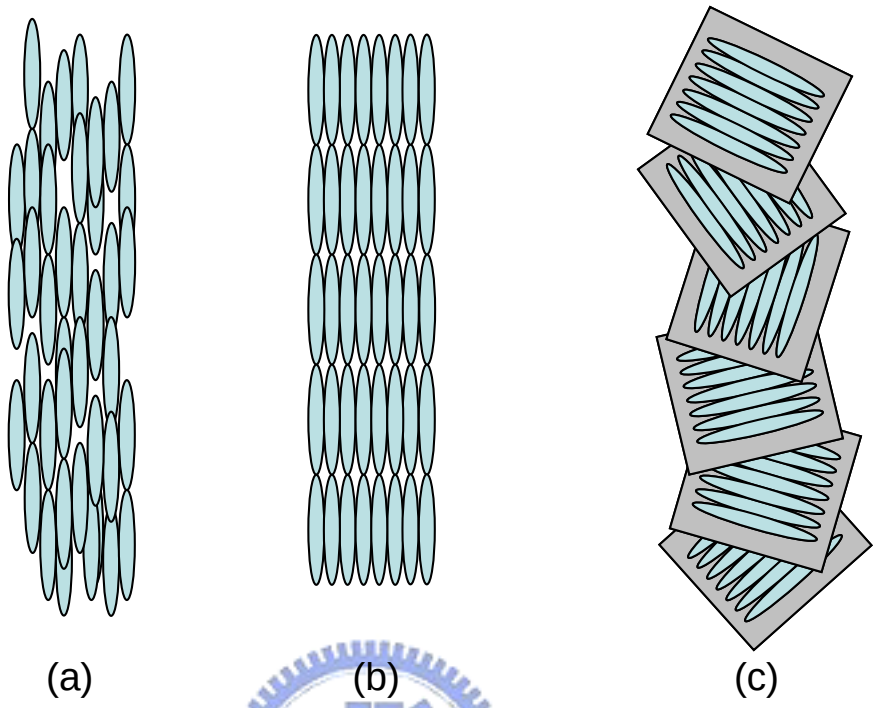

Fig. 1.1 Types of rod-like liquid crystals. (a) Nematic liquid crystal. (b) Smectic liquid crystal (A type). (c) Cholesteric liquid crystal.

I. Nematic

The nematic phase is the simplest of liquid crystal phases and is close to the liquid phase. It is characterized by molecules that has no positional order as in a liquid phase but has tenancy to point toward a same direction vector **n** which is called the director and represents the statistically preferred direction. The molecules are aligned in parallel lines, but not in layers. The optical properties of nematic liquid crystals are similar to uniaxial crystals. The order parameter is the measurement of the degree of order in nematic phase.

$$S = \left\langle \frac{3}{2}\cos^2 \omega - \frac{1}{2} \right\rangle \qquad (1.1)$$

where ω is the deviation angle of each molecule from the director. When S=0, it means the substance is in isotropic phase. S=1 means the substance is in solid state.

II. Smectic

The smectic phase is close to the solid phase. Smectic liquid crystal molecules have one more degree of orientational order than nematic liquid crystal molecules. The molecules parallel to one another, forming a layer, but within the layer no periodic pattern exists. The liquid crystals are ordered in layers and normally float around freely inside these layers. The molecules tend to arrange themselves in the same direction. There are several different sub-phases to describe smectic phase. The two best known of these are smectic A and smectic C. In the smectic A phase, the molecules align perpendicular to the layer planes, and in the smectic C phase the alignment of the molecules is at some arbitrary angle to the normal.

III. Cholesteric

In the cholesteric phase, the molecules are parallel and the layers are arranged in a helical, or spiral, fashion. The cholesteric liquid crystal phase is also called the chiral nematic liquid crystal phase. The name is historic as it goes back to the substances on which Reinitzer made his discovery. The molecules have the chiral centers and are in the nematic phase. They arrange themselves into a strongly twisted structure that often reflects visible light in different bright colors which depend on the temperature. They can therefore be used in temperature sensors.

1.3 Liquid Crystal Display (LCDs) Technology

Thin format, compact size, light weight, and high image quality are the desired features of displays. Liquid crystal has all of the special properties described above, especially the property of circular birefringence, so it can be exploited for the purposes of creating flat-panel displays. A liquid crystal display (LCD) is a thin, flat display device which consists of number

of color or monochrome pixels arrayed in front of a light source or reflector. Nowadays, LCD played a relevant role in display industry.

Generally, a thin film of liquid crystal is placed between two pieces of glass or transparent plastic, which are manufactured with transparent electrodes (typically comprises of indium tin oxide) that make it possible to apply an electric field across small areas of the film of liquid crystal. Polarizers are placed on one or both sides of the glass to polarize the light entering and leaving the crystal. The alignment at the surfaces determines the orientation of the liquid crystal molecules before applying an electric field. Because the liquid crystal material is birefringent, light passing through one polarizing filter is rotated by the liquid crystal helix as it passes through the liquid crystal layer, allowing it to pass through the second polarized filter. When the electric field is applied across the electrodes, the liquid crystal adjusts the polarization. A torque impacts the liquid crystal molecules that reduce the rotation of the polarization of the incident light, and the device appears gray. By controlling the voltage applied across the liquid crystal layer in each pixel, light can be allowed to pass through in varying amounts, correspondingly illuminating the pixel.

The twisted nematic (TN) is the most popular LCD mode, because it provides a high contrast ratio, analog grey scale and low driving voltage. Super-twisted nematic (STN) mode is a type of monochrome passive matrix liquid crystal display (LCD) and STN displays provide more contrast than TN displays by increasing the twist angle of liquid crystal molecules from 90° to 240°. When in in-plane switching (IPS) mode, the liquid crystal molecules rotate in-plane under the applied electric field. The IPS mode shows wider viewing angles than the TN mode. The multi-vertical alignment (MVA) mode can achieve wide viewing angle, too. The MVA mode has homeotropic initial alignment, and the liquid crystal molecules incline to four directions by application of electric field. [3] The optical compensated bend (OCB) mode is

developed for faster response time and wider viewing angle. It will be explained completely in next section.

1.4 Pi-cell and Optical Compensated Bend Mode (OCB)

The pi-cell is generally considered to be the fastest electro-optic response nematic liquid crystal device. [4] Together with the biaxial compensating film, this pi-cell is later improved and is also called the optical compensated bend (OCB) liquid crystal display. [5] The device comprises of parallel-rubbed alignment layer and nematic liquid crystal. It is aligned in splay state and operated in the bend state. The bend and splayed states are not topologically similar, so a nucleation process is required before the pi-cell can be operated. It typically takes a few seconds, and can be unreliable over large areas. The pi-cell has faster switching times than conventional nematic liquid crystal devices, capable of a combined on-off response time of fewer than 5 ms, due to lacking of backflow during director reorientation. It will be explained completely in Chapter 2.

1.5 Motivation and Objective

The need of splay to bend transition is a disadvantage of pi-cells. Techniques for fast splay to bend transition have received increasingly attention. Although aforementioned techniques successfully induced bend transition, most of the techniques sacrifice contrast ratio of the devices. In this study, we present a novel method to form bend transition cores which can spread uniformly in each pixel without the loosing of optic efficiency.

1.6 Organization of This Thesis

The rest of this thesis is organized as follows. Chapter 2 shows overview of pi-cells. Chapter 3 describes the measurement systems adopted in this experiment. The experimental processes,

results, characteristics measurement and performance evaluation are in Chapter 4. The discussions of the results are also brought up in the end of Chapter 4. Conclusions are finally drawn in Chapter 5 along with future research directions pointed out.

Chapter 2

Overview of Pi-Cells

2.1 Introduction

The pi-cell is first introduced by P. J. Bos et al. and was modified into optical compensated bend mode (OCB) by T. Uchida. [4, 5] It is generally considered to be the fastest electro-optic response nematic liquid crystal device due to lacking of backflow during director reorientation.

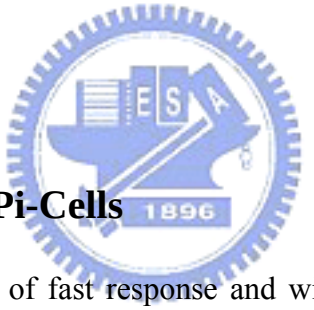

2.2 Characteristics of Pi-Cells

The pi-cell has the advantages of fast response and wide viewing angle. The liquid crystal geometry and the commonly known states in parallel-rubbed nematic device are shown in Fig. 2.1. There are five important configurations in pi-cell operation: the splayed ground state (H), the symmetric splay state (Hs), the asymmetric splay state (Ha), the bend state and the 180° twist state. [6, 7, 8]

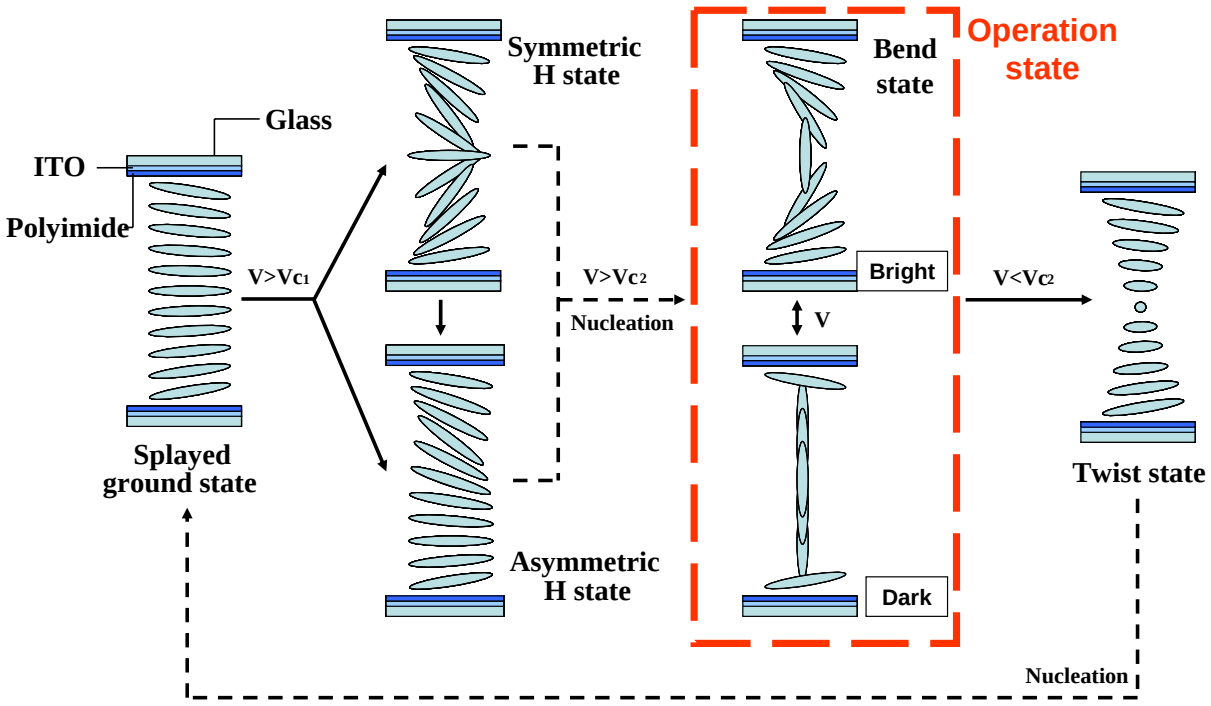

Fig. 2.1. Five configurations of pi-cell. Dotted lines indicate nucleation processes.

If there is no voltage applied, the most stable state is splayed ground state. The H state is a transient state that forms during sudden voltage above a critical voltage, V_{C1} which is around 1 V_{rms} for most materials, applied to the splayed ground state. If the director tilt angle on both surfaces is identical, the device switches into the Hs (symmetry splayed) transient state. Any imbalance of surface tilt results to Ha (asymmetry splayed) transient states. As the voltage is further increased to above a critical voltage V_{C2}, which is around 2 V_{rms} for most materials, the bend state becomes more stable state. The bend state is topologically distinct from the splay state and its transient states. To achieve the uniform bend state from splay state, nucleation process is required and the process will takes few seconds to minutes to complete. If the voltage is fall below V_{C2} the device will relax to the twist state and further nucleation into the splayed ground state.

In the conventional twisted nematic devices, the relaxation times to the twisted state are too long by the backflow-induced alignment phenomenon. [9] The pi-cell eliminates the adverse

effects of flow alignment. In the pi-cell, the surface pre-tilt direction is the same on both surfaces. The surface alignment causes the flow which produces no backwards torque on the director near the center of the cell. The phenomenon is explained by Van Doorn [10] using the numerical solution of the Ericksen-Leslie equations [11], and the mechanism of the fast response was simulated. [12] The symmetry of the pi-cell allows for certain simplification when calculating director dynamics and the switching speeds of positive and negative dielectric anisotropy surface mode devices can be observed. [13] Figure 2.2 shows the torque which induces by the flow accelerates the relaxation.

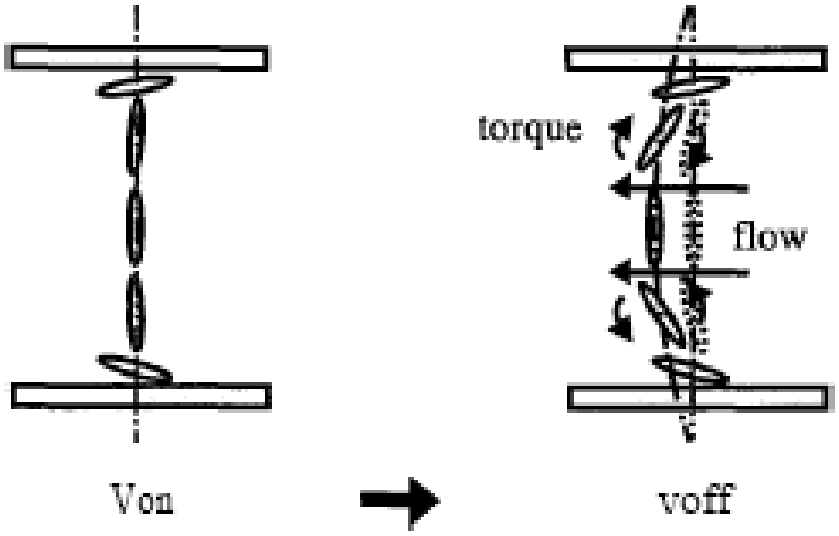

Fig. 2.2. Schematic figure of the dynamics in the pi-cell. The flow induces the torque to accelerate to relax. [12]

Another advantage of the pi-cell is wide viewing angle. Because of the complicated alignment structure, the TN mode LCD is difficult to compensate the birefringence. The uniform optical uniaxial media can be compensated well such as liquid crystals aligned uniformly. When the voltage applies, the degree of bending of the liquid crystal director and its overall birefringence modify. By using various optical films, it can be compensated to obtain a wide viewing angle.

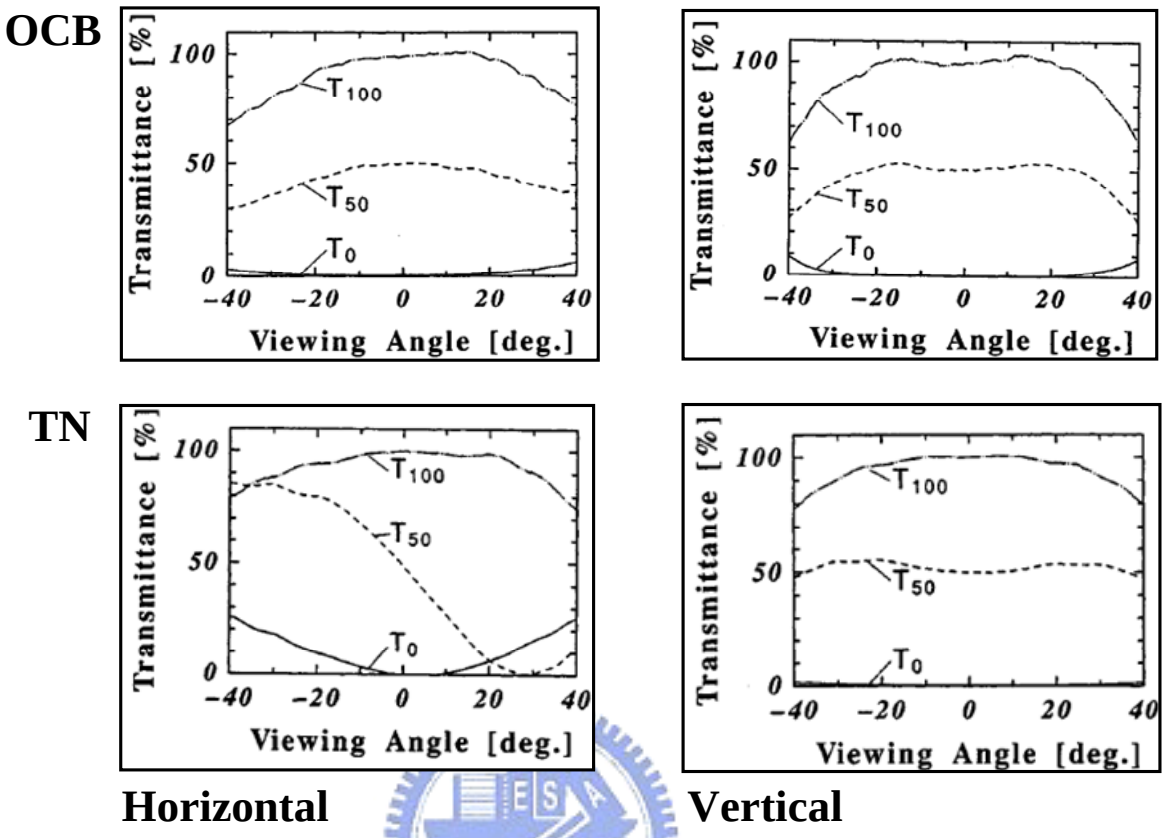

Fig. 2.3. Experimental results of the viewing-angle-dependent transmittance for TN cell and OCB cell. [5]

2.3 Nucleation

In this section, the nucleation process is explained. It is found that the transition is divided into two stages. [14] It shows that the generation of a bend core is essential. [15, 16]

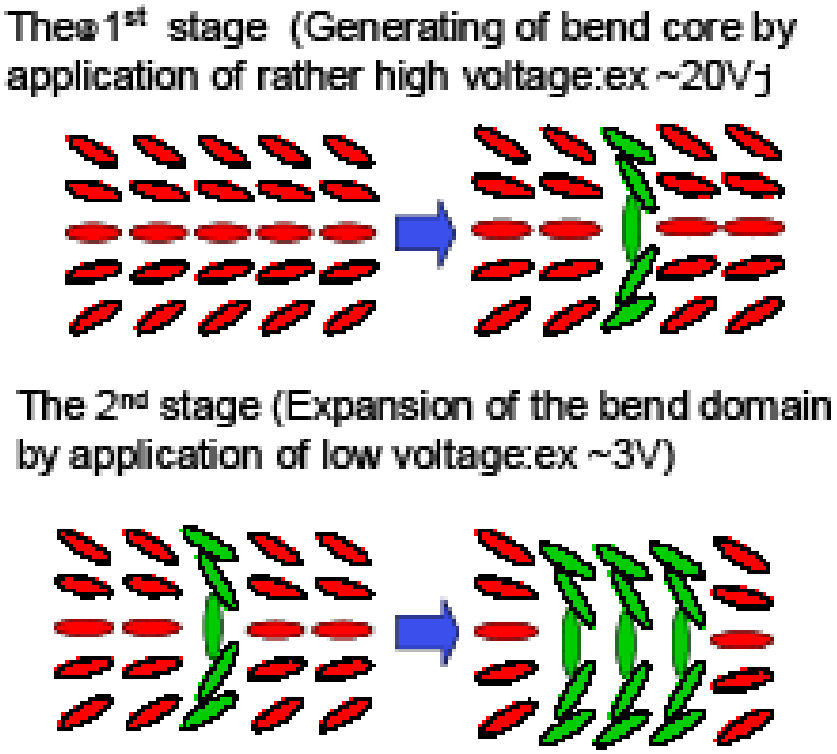

Fig. 2.4. Mechanism of bend transition. [14]

When no voltage is applied, the pi-cell is in the splayed ground state, where the liquid crystal molecules are all aligned with the rubbing direction. By applying a high voltage across the cell, the splayed ground state must be switched into an operating bend state. Because of the different between these states on topology, the transition starts with breaking the anchoring symmetry at the cell surfaces and forming a bend domain with a disclination loop around it. The transition is through the nucleation and movement of disclination lines. In the simulation by P. J. Bos *et al*., it clearly demonstrate it. [16] After the region of concentrated splay distortion is formed, the order parameter starts to decrease in that region. Each of the original defest cores evolve to a pair of -1/2 and +1/2 disclination lines moving away from each other toward other defect lines with the opposite sign as Fig. 2.5 shown. Two portions of the disclination loop that run perpendicular to the rubbing direction are regarded as a pair of wedge disclination lines. The bend nucleation process, which is associated with the liquid crystal physical properties and the cell fabrication process parameters, is relatively easy to

observe the movement of the disclination lines as a growth rate of bend domains under different conditions.

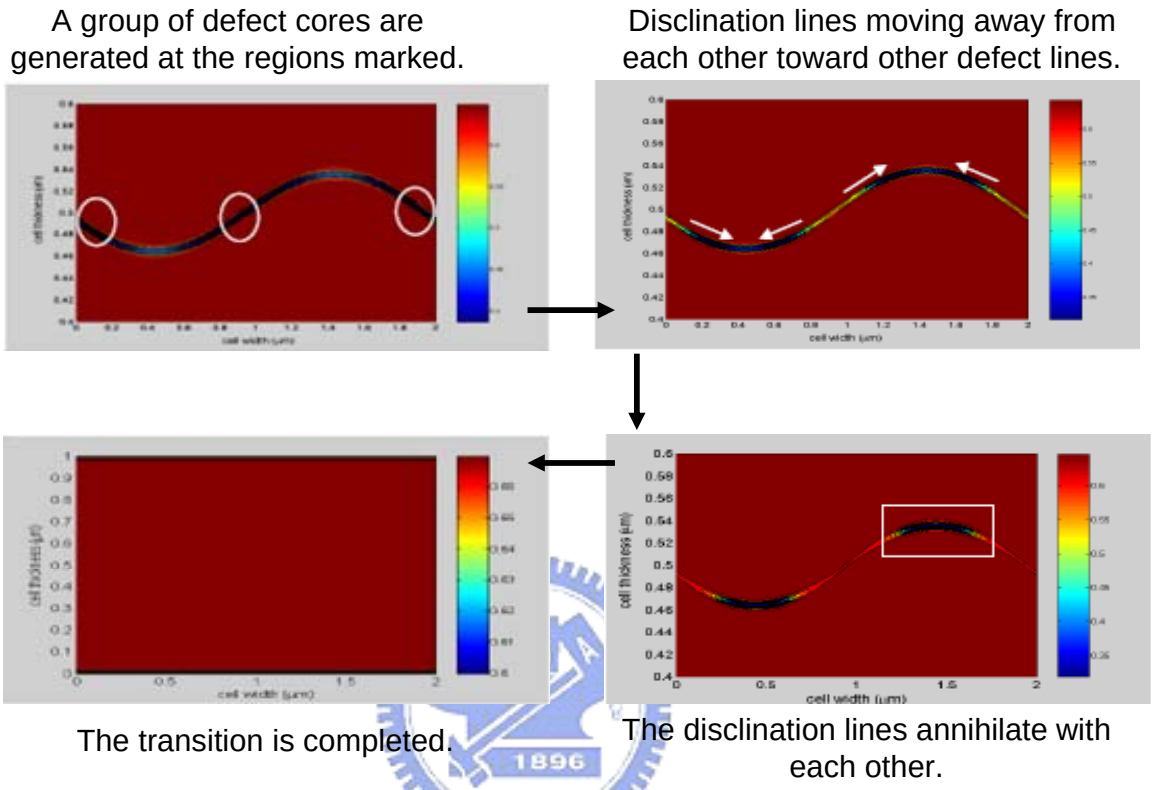

Fig. 2.5. Order parameter profile of simulation. [16]

J. Cheng *et at.* studied the switching process between the bend state and the splay state in a bistable nematic device. [17, 18] The energy difference of the two states can be obtained in a simple formulation, assuming a "boundary-layer model." The "damping factor" is a rate parameter and the value can be determined by the extent of the director disorder around the disclination lines. The velocity of the disclination lines motion can be calculated from the energy difference and the damping factor. The topology of the cell is varied from the splay state to the bend state, and the declination lines finally annihilate with each other when the transition is completed.

2.4 Preliminary Study of Nucleation

Because the bend state is the operation state in pi-cell, many nucleation techniques have been proposed to induce splay to bend transition. These methods can be categorized into chiral and non-chiral doped LC systems.

I. With chiral doping LC systems

For chiral doping LCs system, chiral doping molecules were utilized to stabilize a 180° twist configuration to eliminate the required bend nucleation.[19, 20] The technique eliminates the requirement for nucleation of bend state by using the 180° twist configuration is similar to the bend state at high voltage. Further enhancement with slits and protrusions on the substrates can be seen in Dual-Domain Bend Mode (DDB Mode) LC devices. [21]

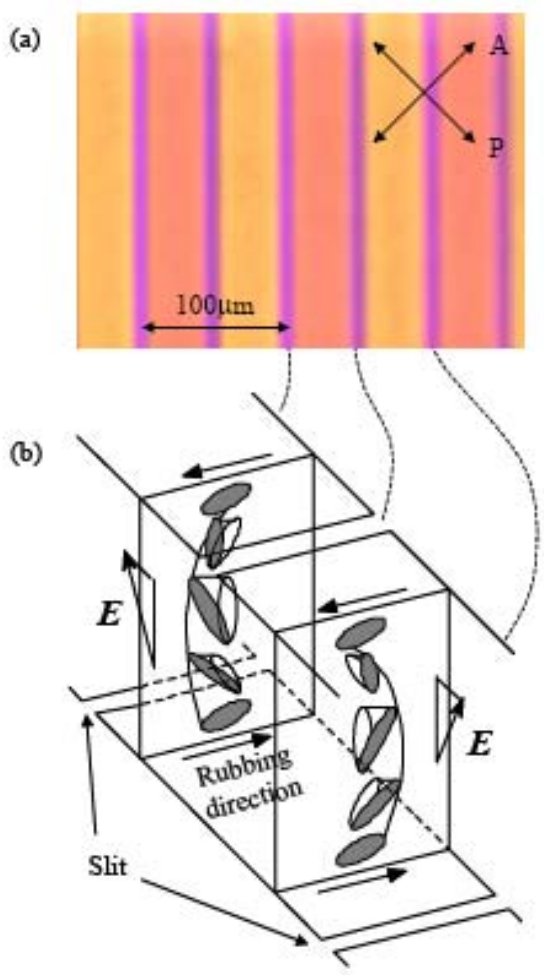

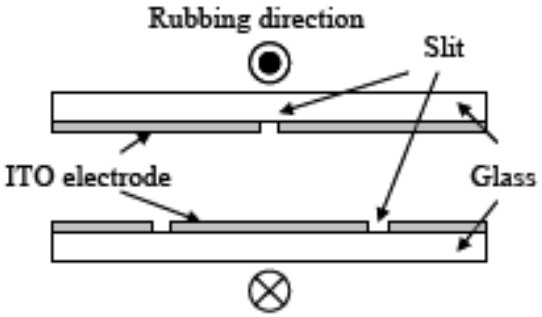

(c)

Fig. 2.6. (a) Microscopic image of DDB cell. (b) Schematic diagram of the director profile of each domain. (c) Cross-sectional structure of DDB cell. [21]

II. Without chiral doping LC systems

Voltage nucleation and stabilization is the basic method for nucleation by using a high voltage (>10V). But it is not suitable for TFT-drivers. [22, 23] On the other hand, the non-chiral doping system is stressed on creating bend transition cores to reduce transition time in pi-cell. Bend transition cores can be generated by defects and structures such as spacers. [24] Under application of a voltage, anisotropic structures around the spacers by adsorption are able to nucleate the bend state. High surface pre-tilt angles were used to stabilize the bend state at 0V as Fig. 2.7 shown. [25, 26] The alignment layers of about 45° pre-tilt angles make pi-cells in the bend alignment with no bias voltage. [27, 28, 29] The relaxation times are increased and the electro-optic modulation is reduced at high surface tilt angles. As the result, the multi-domain alignment method is accessed. [14, 30, 31, 32] In this method, the transition cores are created by high tilt angle alignment region as Fig. 2.8 shown.

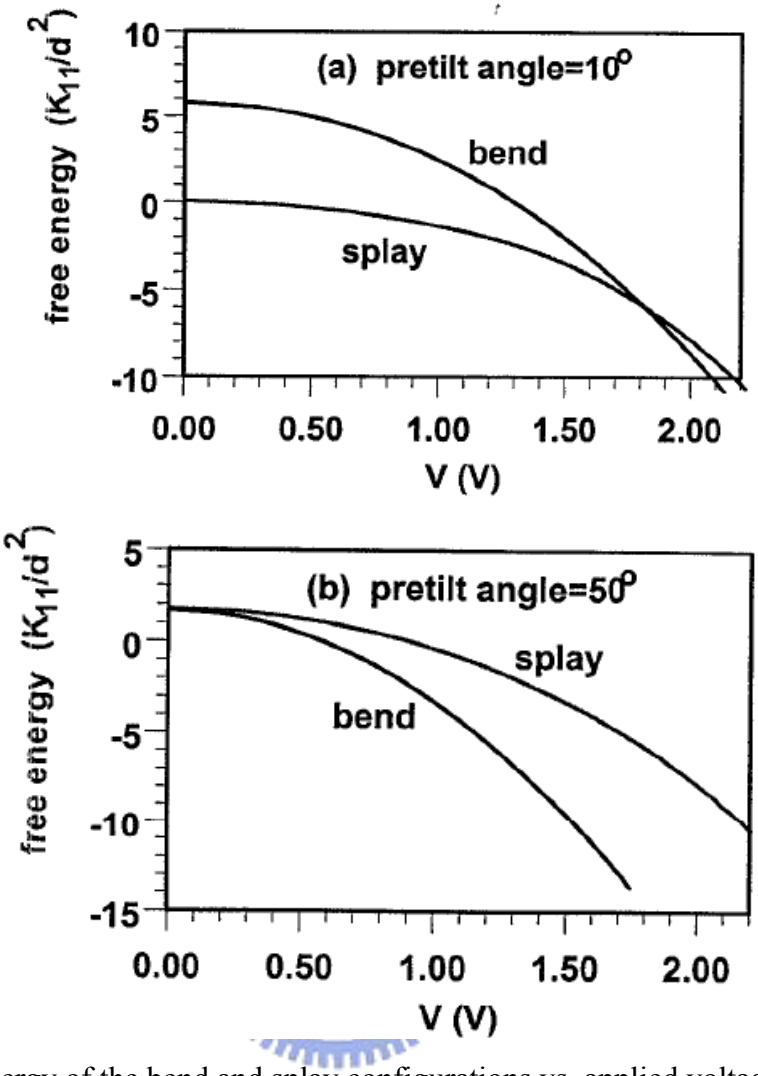

Fig. 2.7. Free energy of the bend and splay configurations vs. applied voltage in the pi-cells. [25]

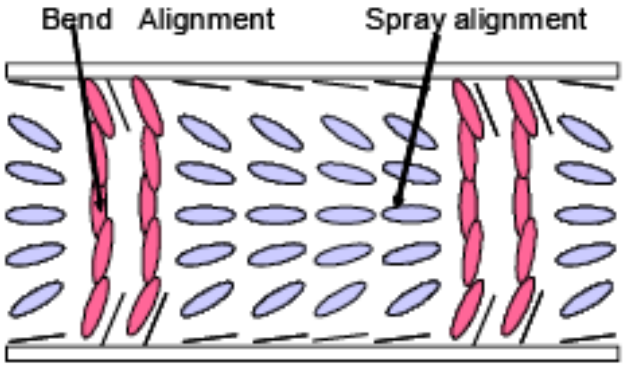

Fig. 2.8. The scheme of liquid crystal alignment of the cell. [14]

Network polymerization is a method to prevent the return of the splay state at low voltages. [33, 34] With polymer walls, an initial splay-to-bend transition is unnecessary. But it is difficult to overcome the ionic contamination and possible image sticking.

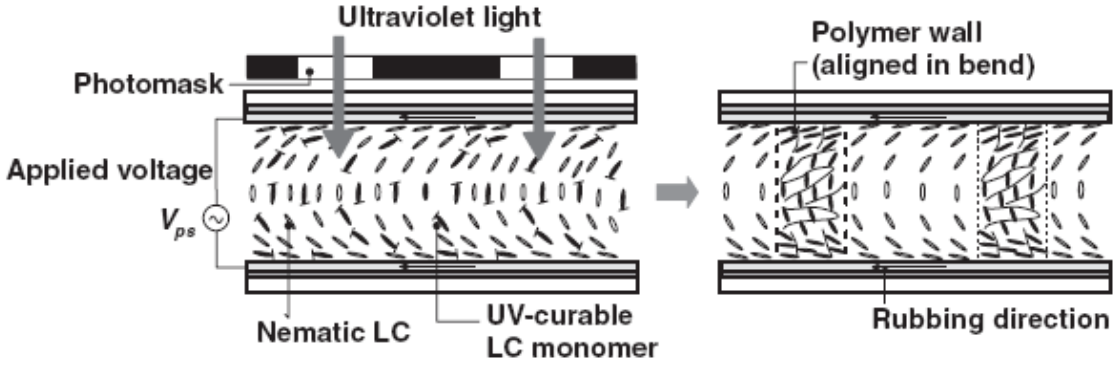

Fig. 2.9. Schematic diagram of polymer wall. [33]

2.5 Summary

We have introduced the pi-cell and the nucleation process. In this study, we present a novel method to form bend transition cores which can spread uniformly in each pixel without the loosing of optic efficiency. This method can achieve fast and uniform transition.

Chapter 3

Measurement Systems

3.1 Introduction

The instruments which are available to characterize the parameters of liquid crystal test cells will be introduced in this chapter. The surface morphology was inspected by atomic force microscope (AFM). After making an empty cell, the cell gap was measured by interferometric method. Instruments such as polarizing optical microscope (POM), and laser optical system were utilized to characterize textures, and electro optical characteristics, respectively. The major features of the above mentioned instruments will be illustrated in the chapter.

3.2 Atomic Force Microscope (AFM)

The atomic force microscope (AFM) consists of a flexible micro-scale cantilever with a scanning sharp tip at its end that is used to scan the specimen surface. The cantilever is typically silicon or silicon nitride with a tip radius of curvature on the order of nanometers. The tips typically have an end radius of 2 nm to 20 nm, depending on tip type. When the tip is brought into proximity of a sample surface, forces between the tip and the sample lead to a deflection of the cantilever according to Hooke's law. Depending on the situation, forces that are measured in AFM include mechanical contact force, Van der Waals forces, capillary forces, chemical bonding, electrostatic forces, magnetic forces, Casimir forces, solvation forces etc. Typically, the deflection is measured using a laser spot reflected from the top of the cantilever

into an array of photodiodes.The scanning motion is conducted by a piezoelectric tube scanner which scans the tip in a raster pattern with respect to the sample (or scans to the sample with respect to the tip). The tip-sample interaction is monitored by reflecting a laser off the back of the cantilever into a split photodiode detector. By detecting the difference in the photo-detector output voltages, changes in the cantilever deflection or oscillation amplitude are determined. The schematic diagram of this mechanism is depicted in Fig. 3.1.

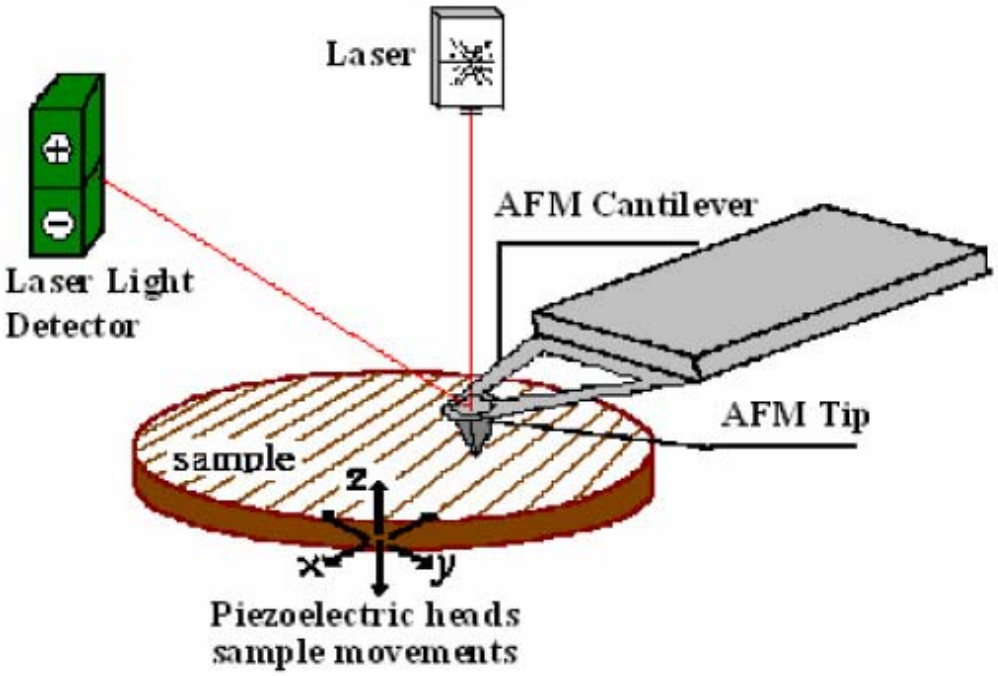

Fig. 3.1. Concept of AFM and the optical lever.

There three major operation made for AFM：

I. Contact mode

Contact mode is the most common method to operate the AFM. But as the term suggests, the tip and the sample remain in close contact as scanning proceeds at this mode. It consists of scanning the probe across a sample surface while monitoring the change in cantilever

deflection with the split photodiode detector. A feedback loop maintains a constant cantilever deflection by vertically moving the scanner to maintain a constant photo-detector difference signal. The distance the scanner moves vertically at each x, y data point is stored by the computer to form the topographic image of the sample surface. This feedback loop maintains a constant force during imaging, which typically ranges between 0.1 to 100 *nN*.

II. Non-contact mode

Non-contact operation is another method which may be employed when imaging by AFM. The cantilever must be oscillated above the surface of the sample at such a distance that we are no longer in the repulsive regime of the inter-molecular force curve. This is a very difficult mode to operate in ambient conditions with the AFM.

III. Tapping mode

It is the next common mode used in AFM. The cantilever is oscillated at its resonance frequency (typically ~300 *kHz*) and positioned above the surface so that it only taps the surface for a very small fraction of its oscillation period when operated in air or other gases. The laser deflection method is used to detect the root-mean-square (RMS) amplitude of cantilever oscillation. A feedback loop maintains a constant oscillation amplitude by moving the scanner vertically at every x, y data point. Recording this movement forms the topographical image. This is still contact with the sample in the sense defined earlier, but the very short time over which this contact occurs means that lateral forces are dramatically reduced as the tip scans over the surface. The advantage of tapping mode over contact mode is that it eliminates the lateral, shear forces present in contact mode, enabling tapping mode to image soft, fragile, and adhesive surfaces without damaging them, which can be a drawback of contact mode AFM. In this thesis, the tapping mode AFM was used.

3.3 Cell Gap Measurement System

For liquid crystal display, the thickness of cell gap has significant influence in optical performance. Thus, every time before the infection of liquid crystal the empty cell gap must be measured and the interferometric method [35] is used. The measurement instrument is UV/Vis spectrophotometer Lambda 650 from Perkin Elmer, and the principle of this method is introduced as below.

UV/Vis spectrophotometer Lambda 650 Perkin Elmer as shown in Fig. 3.2 is operated in the ultraviolet visible spectral ranges (190 nm – 900 nm) with the resolution $\leqq$ 0.17 nm, and the spectrometer features a double-beam, double monochromator, and ratio recording optical system. The instrument is usable in a wide range of applications as indicated by the performance specifications. Absorption and transmittance of materials can be characterized with Lambda 650, and the large cavern supposes the space for polarizers and other expanded object.

Fig. 3.2. The picture of LAMBDA 650 PerKin Elmer.

The basic concept of the measurement method is based on the interference pattern of the light reflected by a layer with two reflecting surfaces. The illustration is as Fig.3.3. Define the coefficient of reflection R_1 as the ratio of the light reflected by surface 1 to the total incident light on surface 1, and R_2 is the reflection coefficient of surface 2. We assume that the total incident light is $I = \cos \omega t$ and no absorption of light in surface 1 and 2. The total reflected light R is

$$R = R_1 \cos \omega t + \sum_{k=1}^{\infty} R_1^{k-1} R_2^{k} (1 - R_1)^{1+k} \cos \omega (t - k t_0), \qquad (3\text{-}1)$$

where $\omega = 2\pi c n_{gap}^{1/2} / \lambda$ and $t_0 = 2 d_{gap} n_{gap}^{1/2} / c$, c is the speed of light in vacuum, λ is the wavelength, d_{gap} is the thickness of the layer, and n_{gap} is the refractive index of the layer.

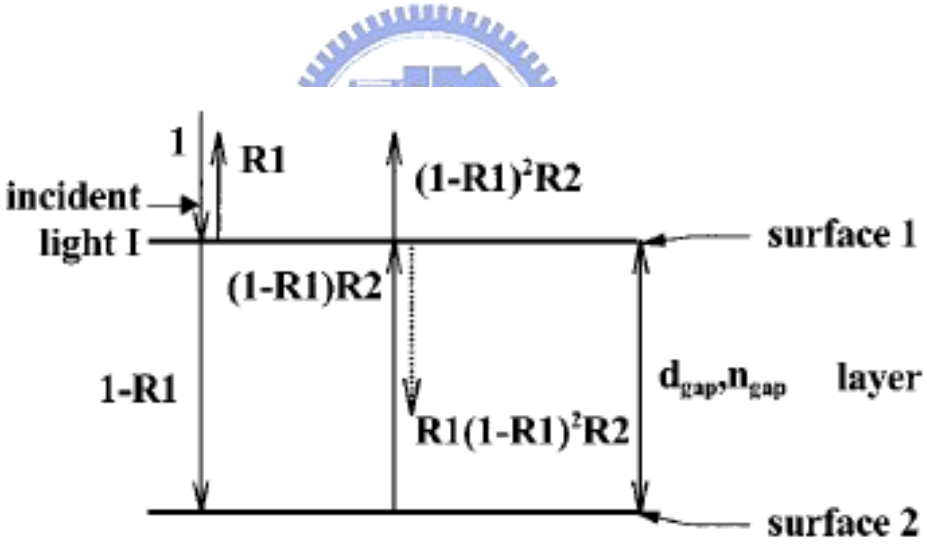

Fig. 3.3. Two reflecting surfaces separated by a layer causing light interference. The dotted line indicates the first internal reflection. [35]

The cosine factors in Eq. (3-1) for k>1 are caused by internal reflections. Since R_1<1 and R_2<1, the magnitude of the cosine factors for k>1 is much smaller than for k=1. Therefore we neglect the internal reflections, so

$$R = R_1 \cos \omega t + (1 - R_1)^2 R_2 \cos(\omega t - \frac{4\pi n_{gap} d_{gap}}{\lambda}) . \quad (3\text{-}2)$$

Thus the reflected spectrum is

$$\left|R(\lambda)\right|^2 = R_1^2 + \left[(1 - R_1)^2 R_2\right]^2 + 2R_1(1 - R_1)^2 R_2 \times \cos(4\pi n_{gap} d_{gap} / \lambda) . \quad (3\text{-}3)$$

The periodic term in Eq. (3-3) causes what is generally known as an interference pattern. The periodicity of the reflected interference spectrum determined the optical thickness of the cell gap, $n_{gap} d_{gap}$.

If for instance λ_1 and λ_2 are two wavelengths yielding extrema in Eq. (3-3), then $\cos(4\pi n_{gap} d_{gap} / \lambda) = \pm 1$ for $\lambda = \lambda_1$ and $\lambda = \lambda_2$. So

$$2n_{gap} d_{gap} = k_1 \lambda_1 / 2 , \quad (3\text{-}4)$$

$$2n_{gap} d_{gap} = k_2 \lambda_2 / 2 , \quad (3\text{-}5)$$

where k_1 and k_2 are the natural numbers. Suppose $\lambda_1 > \lambda_2$, then $k_2 = k_1 + x$, where *x* is a natural number. Then,

$$n_{gap} d_{gap} = \frac{x \lambda_1 \lambda_2}{4(\lambda_1 - \lambda_2)} , \quad (3\text{-}6)$$

and the value of *x-1* indicates the number of extrema in $\left|R(\lambda)\right|^2$ between two wavelength λ_1 and λ_2.

Figure 3.4 shows the measurement of one test cell, and the cell gap was determined from Eq. (3-6).

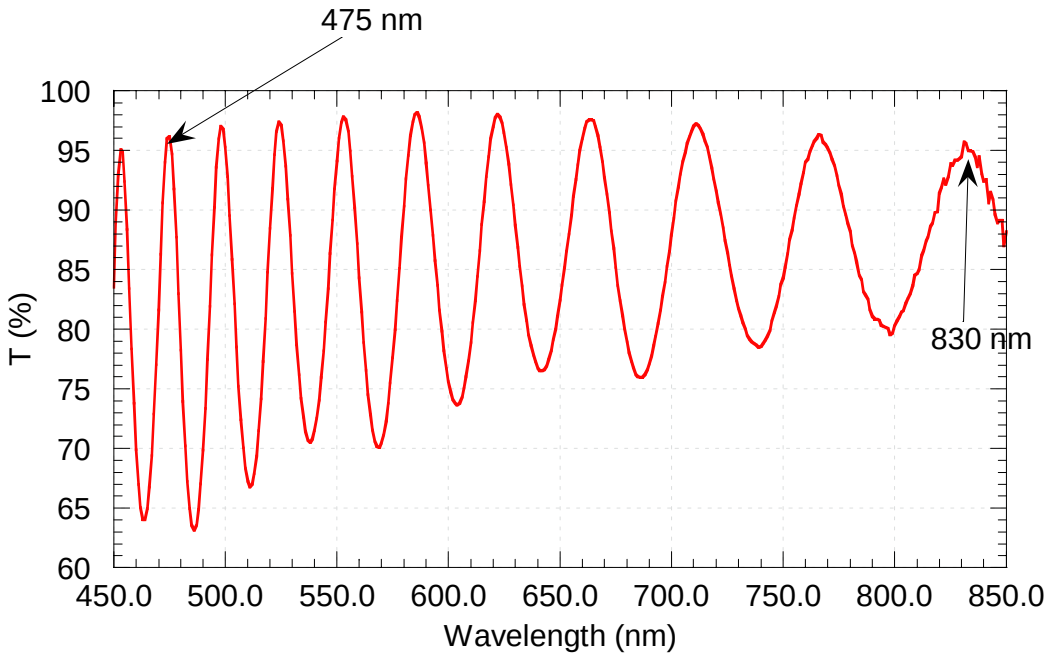

Use the largest possible value for *x*.

$$\frac{x\lambda_1\,\lambda_2}{4\times(\lambda_1-\lambda_2)} = \frac{18\times 830\times 475}{4\times(830-475)} = 4997.54\,(\mathrm{nm}) = 5.0\,(\mathrm{um})$$

Fig. 3.4. Example of a measurement.

3.4 Polarizing Optical Microscope (POM)

The polarized optical microscope is designed to observe and photograph specimens that are visible primarily due to their optically anisotropic character. In order to accomplish this task, the microscope must be equipped with both a polarizer, positioned in the light path somewhere before the specimen, and an analyzer (a second polarizer), placed in the optical pathway between the objective rear aperture and the observation tubes or camera port. Image contrast arises from the interaction of plane-polarized light with a birefringent specimen to produce two individual wave components that are each polarized in mutually perpendicular planes. Liquid crystal microphotographs were observed under POM, Olympus BX51 as shown in Fig. 3.2, the magnifications of POM are 100X, 200X, 500X and 1000X with changeable object lens of 10X, 20X, 50X and 100X, respectively, and a 10X eyepiece. Two

measurable modes depend on transparent and reflective substrates are utilized with bottom light source and top light source, respectively. And adjustable and movable polarizer can be utilized in both modes. Images observed under POM can be captured under CCD, and the parameters such as distance, area and angle can be calculated with its software.

Fig. 3.5. The picture of POM Olympus BX51.

3.5 Laser Optics System

The laser optical system was used for the measurement of electro-optical properties, such as V-T characteristics and response time. This system is shown in Fig. 3.6. The test cell was placed between a polarizer and an analyzer. The light source is He-Ne laser. A 10% ND filter is used for reducing the intensity of laser source to fulfill the intensity within the acceptable range of the photo detector. The test cell was driven by a waveform generator WFG500 from FLC Electronics AB which is connected with computer through GPIB interface. WFG500 is

multi-channel high voltage waveform generator. It is powerful to be a high voltage signal generator with 8 output channels and waveform-designed ability. Any waveforms even they are not regular can be designed with the maximum output voltage for ±100V and the minimum designable pulse width for 200ns. The optical signals were received by photo detector PIN 20 from FLC Electronics AB. The light sensitive component, silicon PIN photo-diode contributes to a good compromise between sensitivity and speed, and the signal with its response more 40ns can be detected by this instrument. The photo detector would transform the intensity of laser light into voltage, and were exhibited with oscilloscope or multimeter.

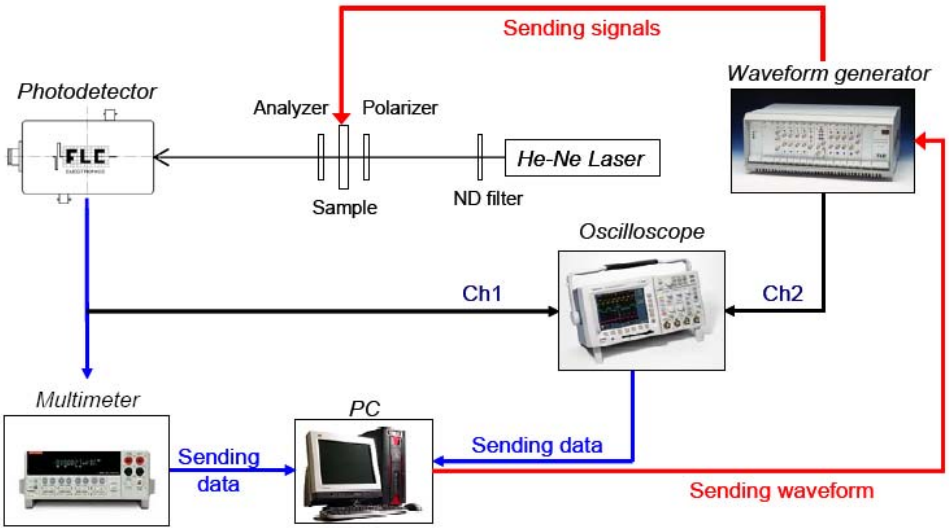

Fig. 3.6. Schematic of the laser optics system.

Chapter 4

Experimental Results and Discussion

4.1 Introduction

It is well known that the operating state (bend state) of a pi-cell must be nucleated then uniformly spread the bend orientation in splay state before operation. In this thesis, the random distribution of silicon oxide nano-particles has been investigated for decreasing the time of splay-to-bend transition in pi-cells. The electro-optical properties were characterized under 5 μm test cell with optical system and polarizing optical microscope (POM). Transition time was measured by digital-camera. Under the optimum conditions, the 50% reduction of splay-to-bend transition time was found in nanostructure structure treated surfaces.

4.2 Cell Fabrication Process

The fabrication process of our liquid crystal test cell is shown in Fig. 4.1.

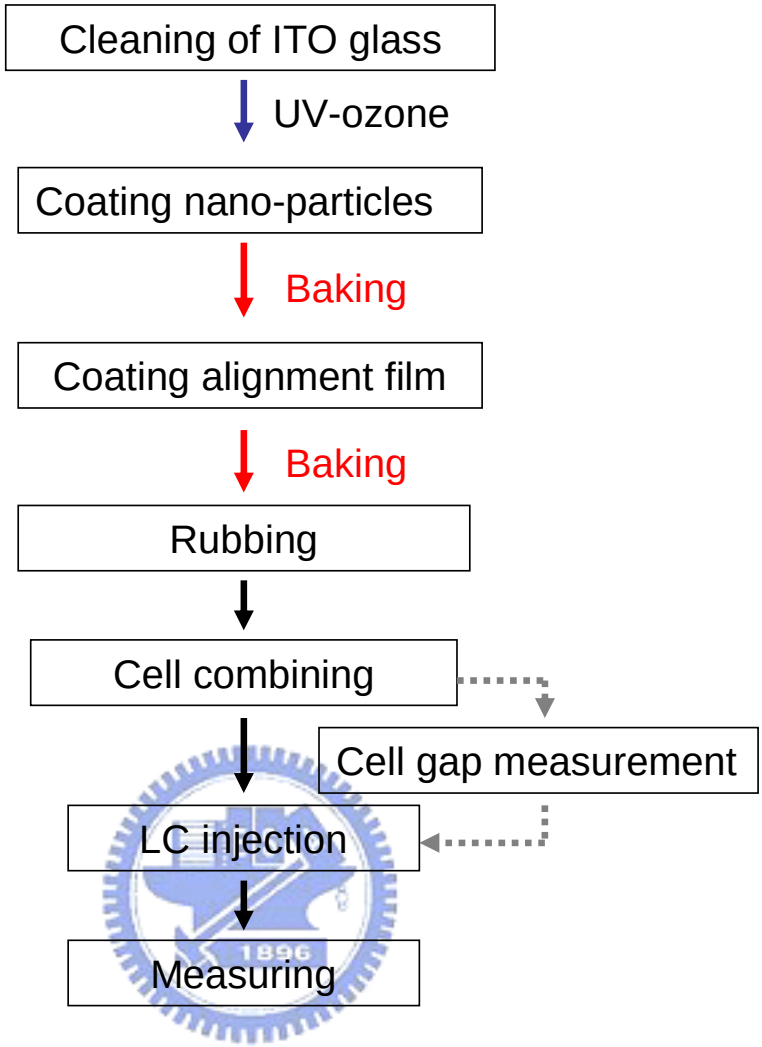

Fig. 4.1. The flowchart of the cell fabrication process.

I. Each piece of glass was rinsed with detergent and rubbed by hands carefully. Then, the glass was washed with DI water until the water flowing along the surface smoothly. After that, the glass was loaded with a holder into DI water and shaken with ultra sonic for 20 minutes. Then, we refilled it with clean DI water and shook it with ultra sonic for 20 minutes again.

II. In order to rip off the water, we blew the surface of glass with nitrogen gas, and then baked for 30 minutes at 110℃. The surface was treated by UV-Ozone for 25 minutes in order to have better hydrophilic and adhesive.

III. The DI water was dropped on ITO glass to cover the whole glass for 60 seconds, and spun. It was for wetter surface and better adhesion of nano-particles solutions. Next, the diluted silicon oxides nano-particles aqueous solutions were dropped on the glass for 60 seconds and spun. The procedure of spin-coating is as Table 4.1.

Table 4.1 The procedure of spin-coating.

	Speed (rpm)	Time(sec)
1st spin	0	60
2nd spin	700	10
3rd spin	5000	60

After spin-coating, the samples were baked in 30 minutes at 110℃.

IV. We coated the alignment layer with the same step in Ⅲ. First, the solvent was used to spin. Then the 50% polyimide solutions were used to spin. After this, the samples were baked in one hour at 220℃. The polyimide was PIA-X201-G01 from Chisso. The film thickness, which was measured by AFM (from Digital Instruments), was about 35nm.

V. In our study, the rubbing method on polyimide for fabrication of alignment layer was used. This method used mechanical force to rearrange the orientation of polyimide film, and then the rod-shape liquid crystal molecule was aligned naturally with the micro-groove of polyimide film surface. The rubbing condition we used was 500rpm for rotation speed, and 1000rpm for table speed.

VI. UV glue, which is NOA-65 from Norland, mixed with about 5 wt% 5um spacer. We dropped a small amount of the mixture at four corner of the bottom plate. Then, the top plate was covered on top of it and pressed uniformly. Then, the cell was placed under a UV lamp to cure the glue. After 5 minutes, an empty cell was done.

VII. The cell gap of an empty cell was measured by UV/Vis spectrophotometer Lambda 650

(from Perkin Elmer). It was explained completely in section 3.3.

VIII. The liquid crystal material, which is ZCE-5096XX from Chisso, was injected from the edge of the cell. The specification of ZCE-5096XX is shown in Table 4.2. We soldered the wire at the ITO contact, and then the test cell was completely done.

Table 4.2. The specification of liquid crystal material ZCE-5096XX.

Sample		ZCE-5096XX
$T_{N->C[S]}$		<-20 ℃
$T_{N->I}$		95.5 ℃
Viscosity η (at 20℃)		46.7 mPa · s
Optical anisotropy (at 25℃ 589nm)	△n	0.158
	n_e	1.662
	n_o	1.504
Dielectric anisotropy (at 25℃)	△ε	10.0
	$\varepsilon_{\parallel}$	14.1
	$\varepsilon_{\perp}$	4.1
Specific resistivity ρ (at 25℃)		$>1.5*10^{14}\Omega \cdot cm$
K_{11}		9.8 dyne
K_{22}		5.8 dyne
K_{33}		11.8 dyne
γ1		178 mPas

4.3 Observation of Surfaces

This study has researched the nano-scale transition cores in the cell, and the nano-particles have been used. There are several methods to achieve the uniform distribution. At first, the

silver nano-particles (mean diameter=25nm) dissolved in isopropylalcoho (IPA) (form SeanDa Technology CO., LTD) which has the mixing ratios 500,000 parts per million (ppm) were used. But this material was not stable, it would be aggregated easily. The attenuate Ag nano-particles solution was coated on ITO glass. The surface image observed by AFM as below. The result couldn't fulfill our requirements, and the material was unstable.

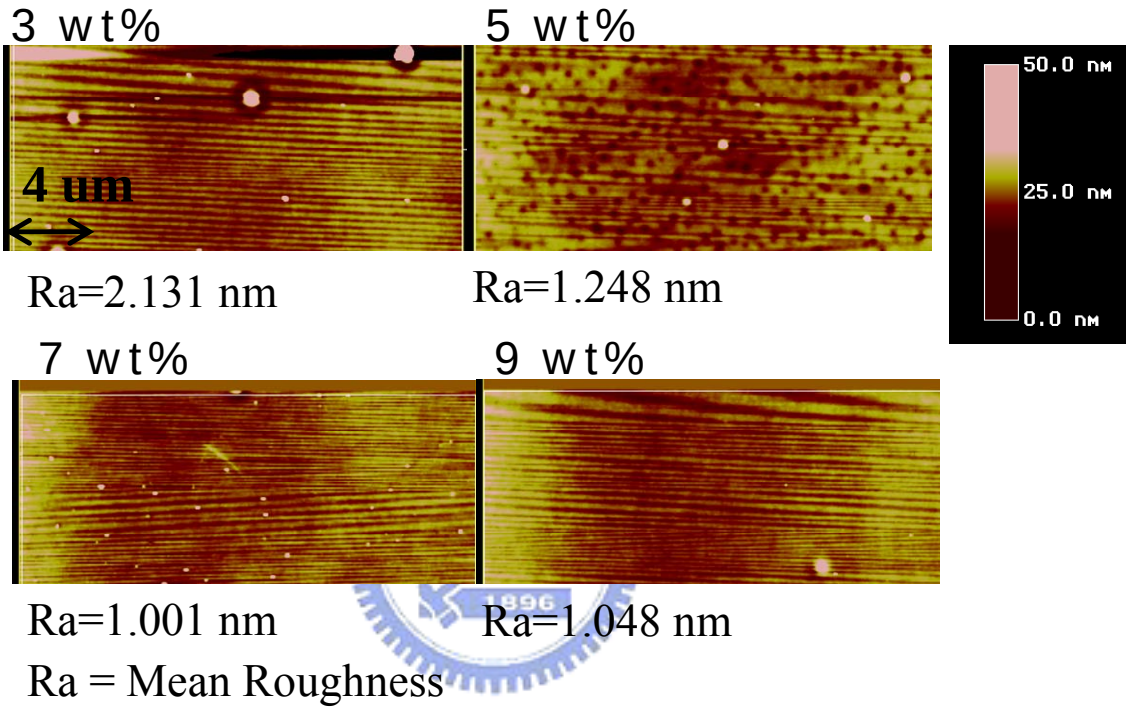

Fig. 4.2. The AFM image of Ag nano-particles surface.

Figure 4.3 describes the transmittance of glasses. The using of Ag nano-particles influences the transmittance seriously. This experiment given above doesn't achieve the aim of creating the nano-scale protrusions and it diminishes the transmittance of the glasses.

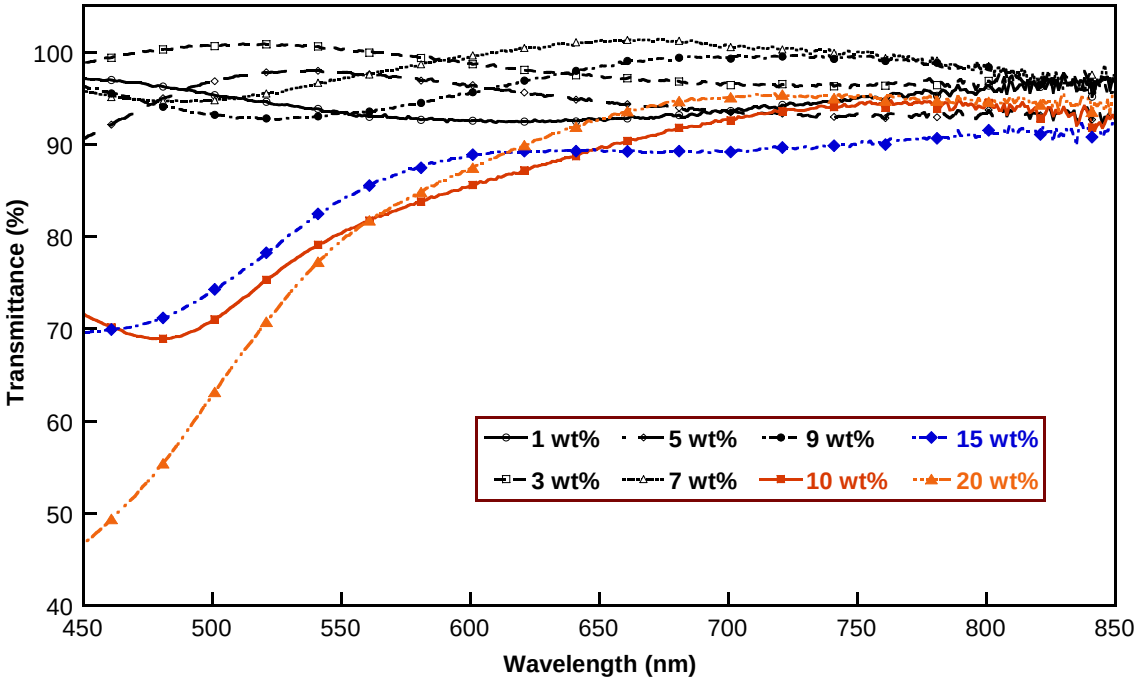

Fig. 4.3. The transmittance of the ITO glasses.

Then, the mixture was considered. The silver nano-particles solution mixing with the solvent of polyimide in 1 and 5 weight percentage was spin-coated on ITO glass substrate before polyimide coating. The observation of AFM is shown in Fig. 4.4. According to this figure, the nano-scale protrusions still did not form clearly.

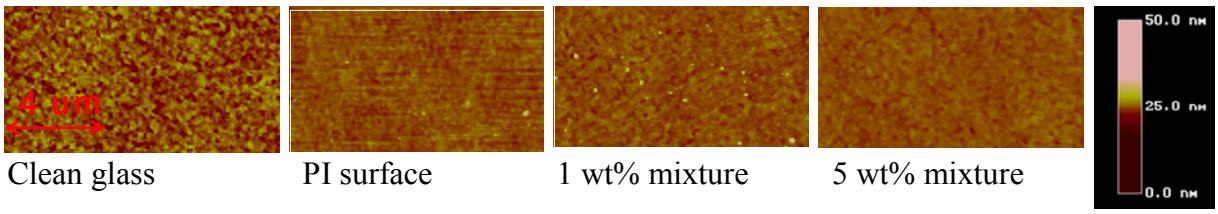

Fig. 4.4. The AFM image of Ag nano-particles mixture surface.

Subsequently, the silicon oxides nano-particles (90 nm, mean diameter, from Everlight Chemical Industrial Co.) diluted in aqueous solutions were used. At first, the solution separated by an atomizer, but the atomizer couldn't decentralize the nano-particles well. The

size of the gibbosities which have the ring shape was too huge for being transition cores as below.

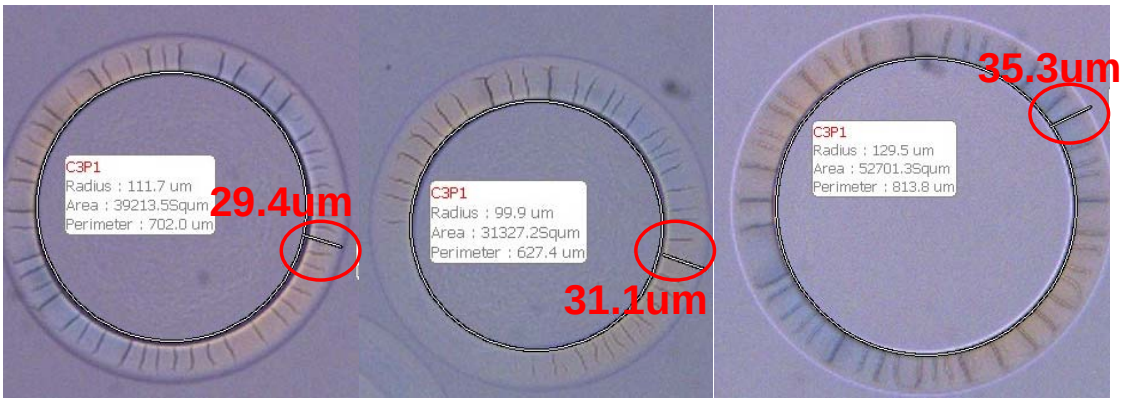

Fig. 4.5. The pictures of atomized nano-particles solutions treated surface taken by POM.

So we used spin-coating method to separate the nano-particles. Silicon oxides nano-particles solution was coated on the ITO glass substrate. Figure 4.7 shows the schematic representation and the atomic force microscopy (AFM) image of the surface of nano-particles with polyimide on top. In general, the 0.004wt% silicon oxides nano-particles in aqueous solutions were applied and the average distribution density is 0.08 μm^{-2}. The diameter of the protrusions is in the region of 200-300 nm, with the height of 150-250 nm.

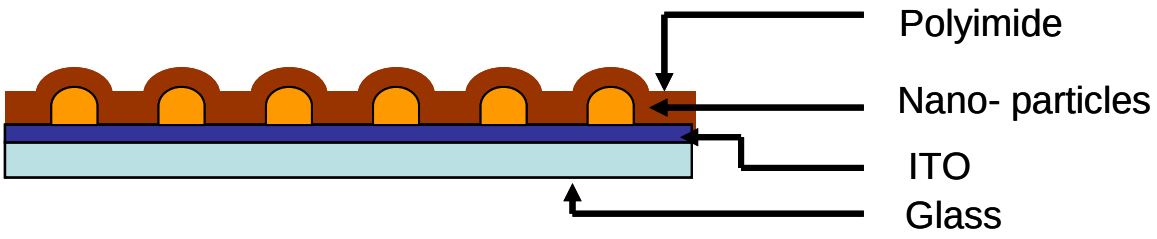

(a)

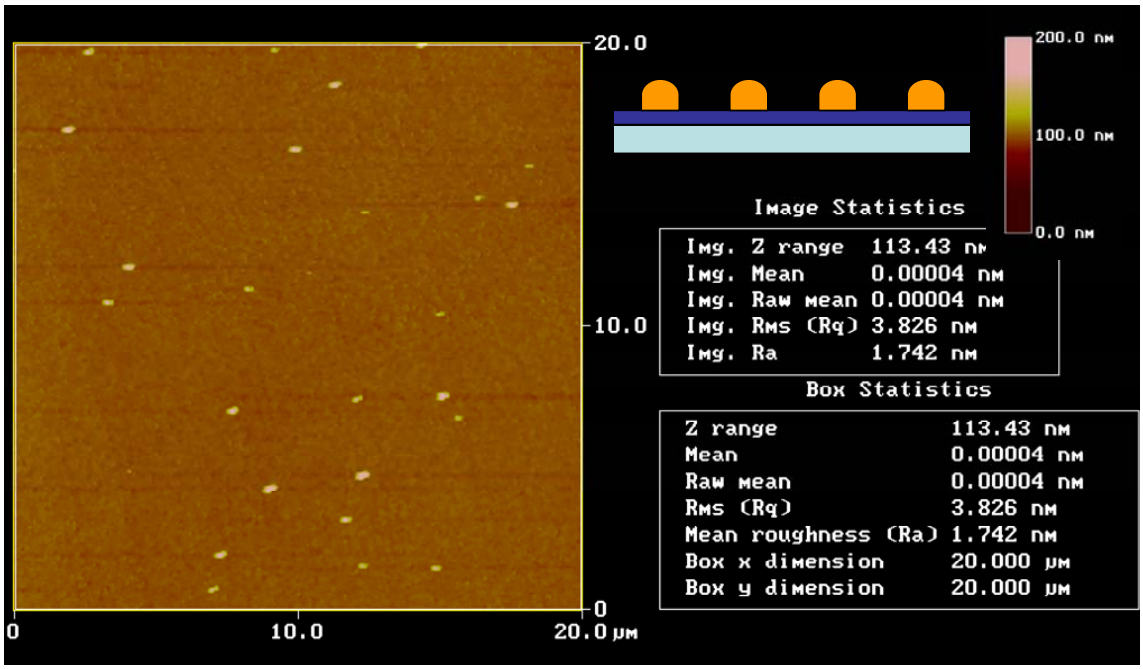

(b)

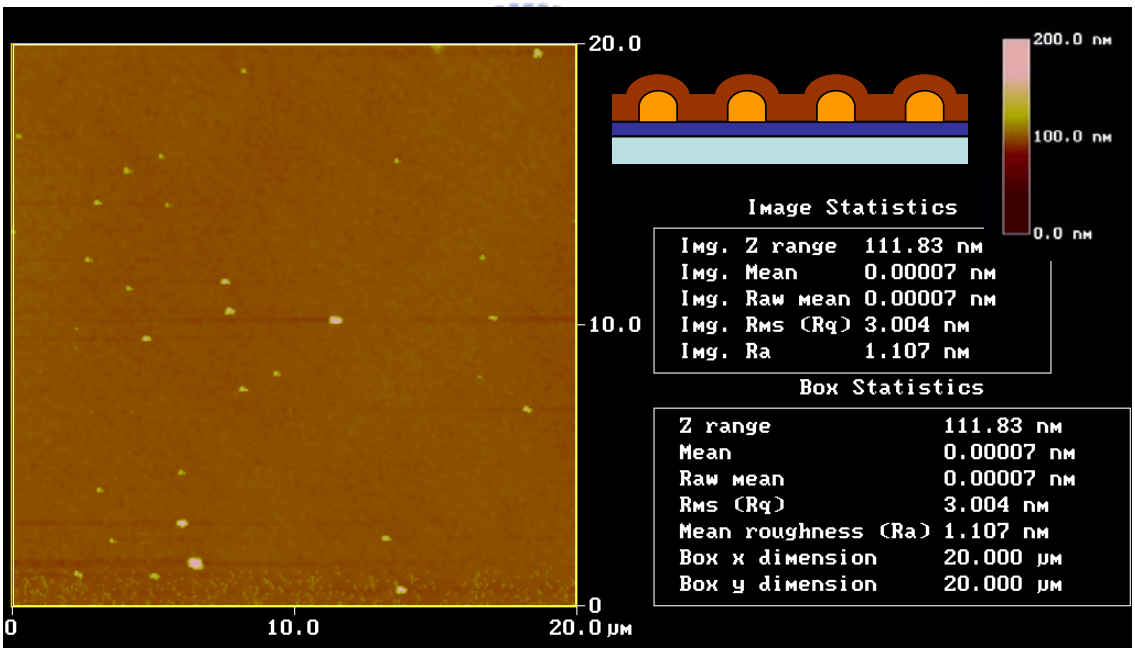

(c)

Fig. 4.7. (a) Schematic illustration of nano-structured surfaces. (b) The AFM image of nano-silicon-particles surface. (0.004wt%) (c) The AFM image of PI surface with nano-particles. (0.004wt%)

4.4 Improvement of Transition Time

In order to observe the transition time by video camera, the lower voltage was applied on test cells. This technique enabled the observation of splay to bend transition. Figure 4.8 shows the pictures of test cell with nanostructure during transition. It could be observed that the transition appeared in circles around the transition cores.

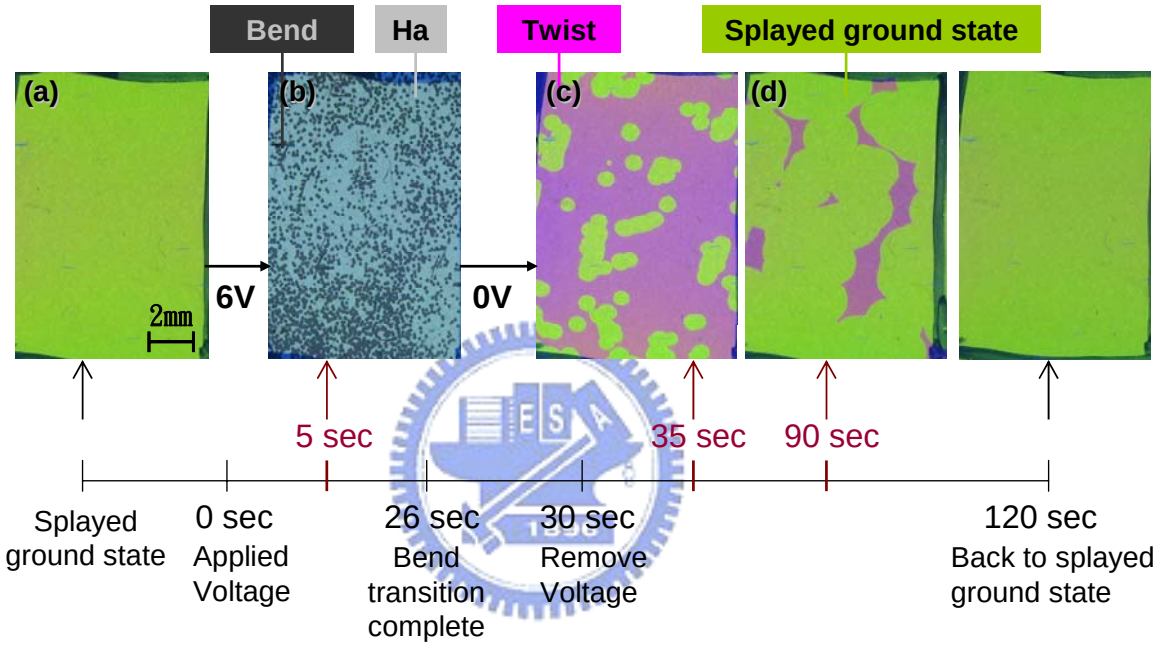

Fig. 4.8. Pictures of test cell with nanostructures during transition taken by digital-camera. (a) is splayed ground state, (b) is in the asymmetric splay to bend transition, and (c)(d) are during twist to splay transition.

Table 4.3 shows the transition time of the test cells (2.5*2cm^2, cell gap=4.9±0.2μm) while applying AC square wave (6V). The transition was counted by the video image captured by video camera. The frame rate was 25 fps (frames per second). The time of complete transition was counted in the film. The Ultra Slim Lightbox (from Microlight Computer Co., Ltd.) which had two CCFL tubes as the light sources was used to be the backlight. Fast bend transition is achieved with the nanostructures treated surfaces. Both transition times between

asymmetric splay state to bend state and twist state to splayed ground state are greatly reduced with this technique.

Table 4.3. The transition time during nucleation.

	Ha->Bend (sec)	Twist->Splay (sec)
w/o nano-structure	52.20	202.26
with nano-structure	46.83	97.82

4.5 Influence of Protrusions Distribution Density

In section 4.4, the nanostructure has significant influence in transition time. It might be better by using higher distribution density. The concentration of nano-particles was changed for different distribution density of protrusions. By using different concentration of silicon oxides nano-particles, the average distribution density of the protrusions varies. When the concentration increases, the density becomes saturation. The trend of the distribution density regarding to the different silicon oxides concentration (Fig. 4.9) and the surface observation images of different concentration by AFM (Fig. 4.10) show as below.

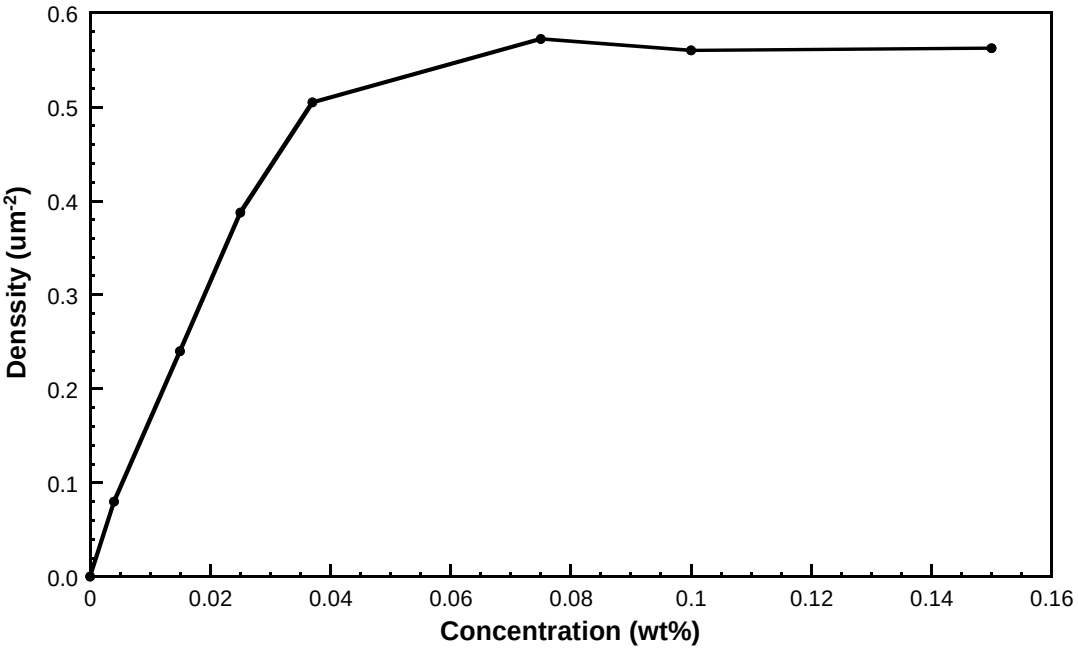

Fig. 4.9. The relation between concentration and density.

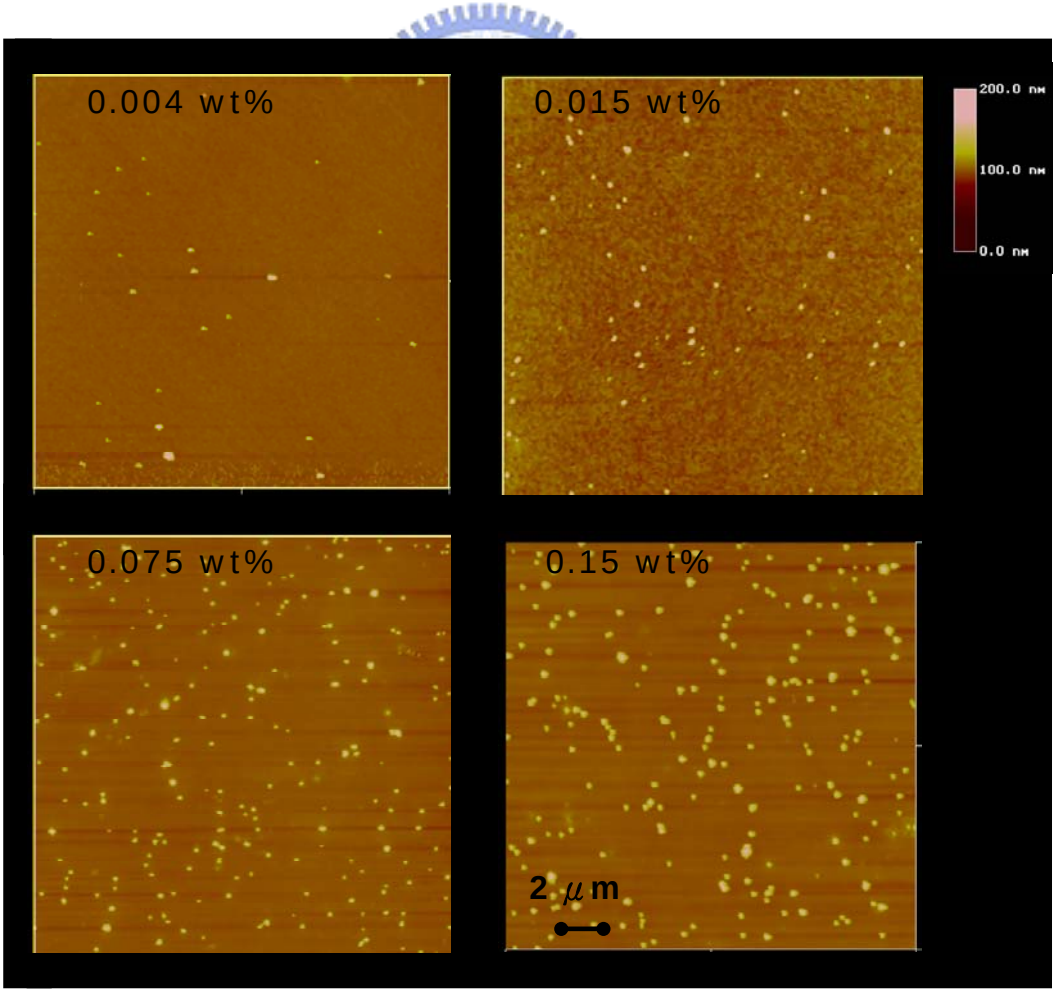

Fig. 4.10. The AFM images of different concentration.

The relation between the distribution density of nanostructures and the transition time shows in Fig. 4.11. The asymmetry splay state to bend state transition time could have 50% reduction with 0.075wt% nano-particle concentration. The higher protrusions distribution density has the less Ha-to-bend transition time.

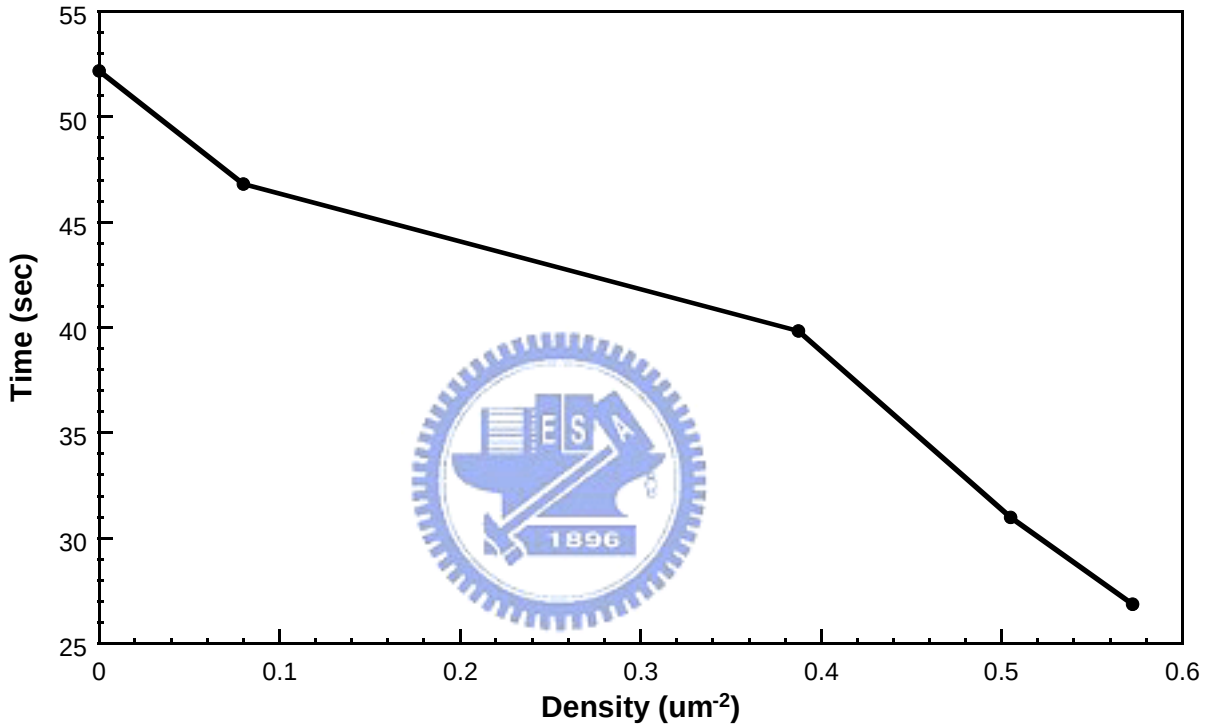

Fig. 4.11. The trend of the asymmetric splay state to bend state transition time regarding to the distribution density.

4.6 Measurement of Electro-Optical Properties

The photographs of the test cells which were taken by polarizing optical microscope (POM) show in Fig. 4.13 In this picture, it shows that the optic efficiency doesn't decrease by using the nanostructures. By the way, in this picture the ON/OFF states of the test cells don't have the best contrast ratio. It can be improved by using optical compensation films.

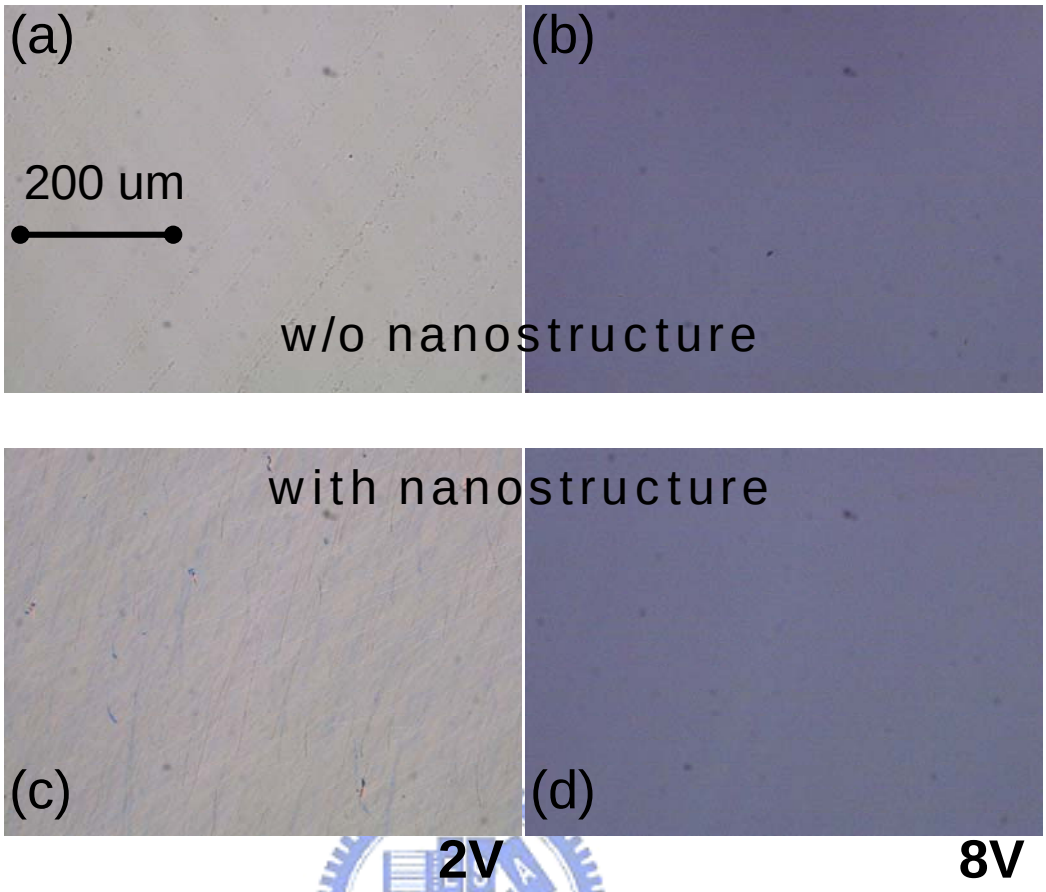

Fig. 4.12. Pictures of the test cells taken by POM. (a)(b) are the ON and OFF state of normal cell, and (c)(d) are the ON and OFF state of cell with nanostructure.

The nano-particles would not impact on transmittance as Fig. 4.6 shown. The results are measured by UV/Vis spectrophotometer Lambda 650. It was explained in section 3.3. The transmittance approached to 100% with the clean ITO glass.

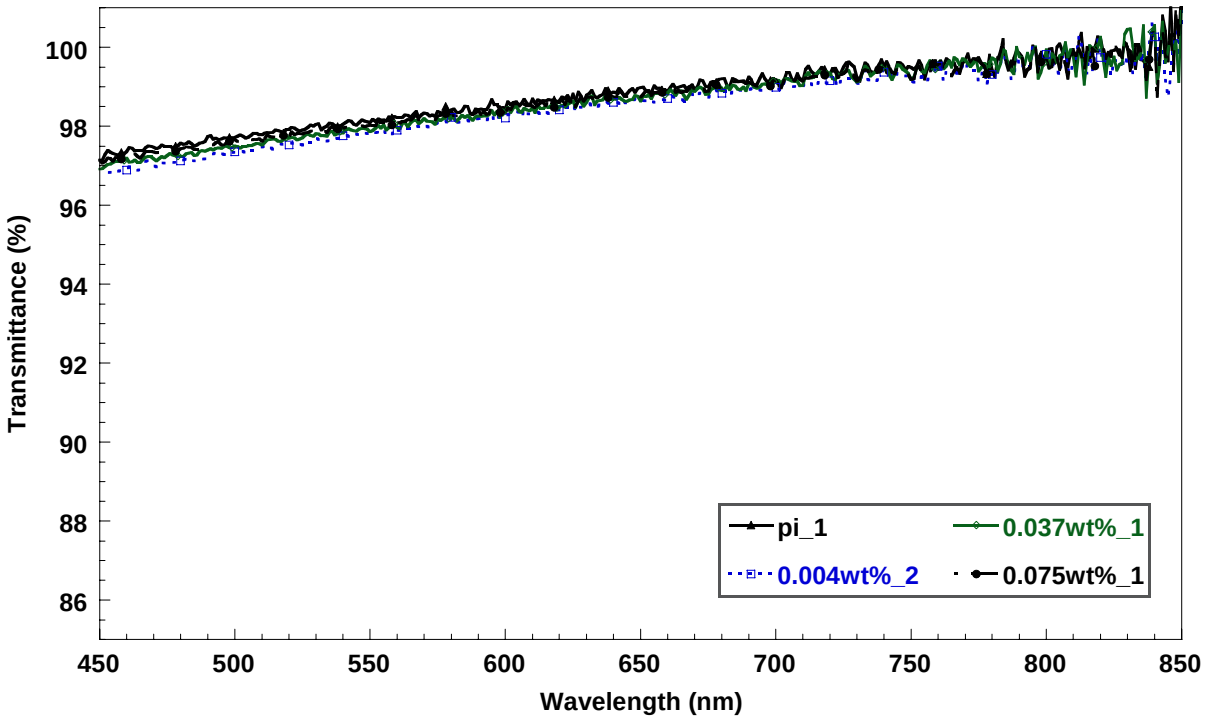

Fig. 4.13. The influence of the nano-particles concentration in transmittance.

The critical voltage is another essential parameter of pi-cells. The voltage isn't influence by the addition of nano-particles shown in Fig. 4.14.

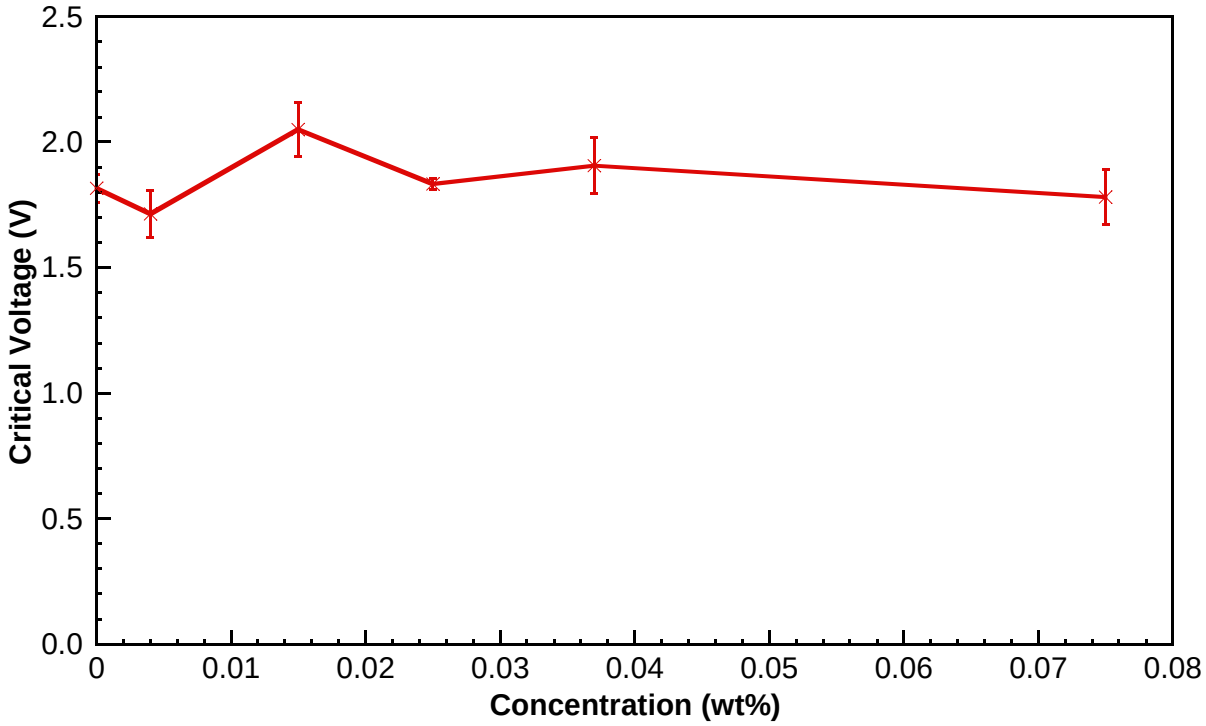

Fig. 4.14. The critical voltage (V_{cr}) of test cells.

The pi-cell is well known to be the fastest electro-optic response nematic liquid crystal device due to lacking of backflow during director reorientation. Accordingly, the response time of test cell would be the most significant parameter. Figure 4.15 shows the measurement result of response time. The nano-structures don't impact on the electro optical characteristics of the pi-cells.

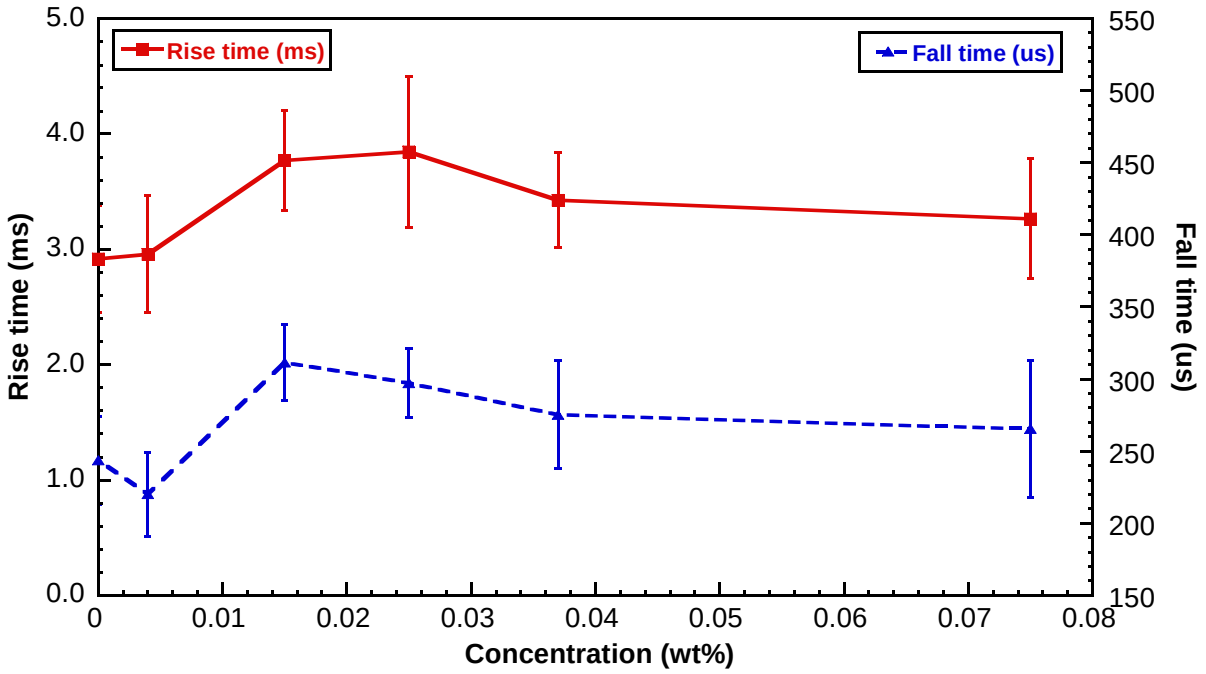

Fig. 4.15. The measurement result of response time.

4.7 Summary

In this study, a nucleation technique for obtaining fast transition to bend state in pi-cells has been achieved. We investigated the random distribution of silicon oxide nano-particles for decreasing the time of splay-to-bend transition in pi-cells. The nano-structure protrusions, which consist of silicon oxides nano-particles, become the bend transition core during nucleation. These nano-structures can effectively reduce the transition time without losing contrast ratio of the devices.

Chapter 5

Conclusions

5.1 Conclusions

Firstly, this study has achieved fast transition to bend state in pi-cells by a nucleation technique. Secondly, the protrusions on substrate, which consist of silicon oxides nano-particles, become the transition cores during nucleation. This technique demonstrated successful fast nucleation. The random distribution of silicon oxide nano-particles can induce fast splay to bend transition. There is a 50% reduction of transition time. And at the end, the nano-structures don't influence the transmittance of the device. The nano-structure can reduce the transition time without losing light efficiency.

5.2 Future work

The nano-structures successfully induce fast and uniform transition in pi-cells without reducing the transmittance of the devices. But more complicated fabrication process was required. We have tried to mixing the nano-particles solution with the solvent of polyimide, but the nano-scale protrusions did not form. If there is a new nano-particle material which can mix with polyimide uniformly, the fabrication process will be simplified. The silicon oxides nano-particles was used in this work, but it can't conduct electricity. If there is a new nano-particle material which can conduct electricity, the result may be better. If the procedure of spin-coating changed, the density of protrusion may be higher than the saturation value

0.56 μm^{-2}. The increasing of density may induce the faster transition. Therefore, the faster transition can be achieved.

References

[1] F. Reinizer, *Monatsh. Chem.*, Vol. **9**, p. 421 (1888)

[2] O. Lehmann, *Z. Physik. Chem.*, Vol. **4**, p. 462 (1889)

[3] K. Takatoh, M. Hasegawa, M. Koden, N. Itoh, R. Hasegawa, M. Sakamoto, *Alignment technologies and applications of liquid crystal devices*, Taylor & Francis (2005)

[4] P. J. Bos, K.R. Koehler/Beran, *Mol. Cryst. Liq. Cryst.*, Vol. **113**, p. 329 (1984).

[5] Y. Yamaguchi, T. Miyashita, T. Uchida, *SID*, 19-04, p. 277 (1993).

[6] E. J. Acosta, M. J. Towler and H. G. Walton, *Liq. Cryst.*, Vol. **27**, p. 977 (2000).

[7] P. D. Brimicombe and E. P. Raynes, *Liq. Cryst.*, Vol. **32**, p. 1273 (2005).

[8] P. D. Brimicombe and E. P. Raynes, *Appl. Phys. Lett.*, Vol. **89**, p. 031121 (2006).

[9] D. W. Berreman, *J. Appl. Phys.*, Vol. **46**, p. 3746 (1975)

[10] C. Z. Van Doorn, *J. Appl. Phys.*, Vol. **46**, p. 3738 (1975).

[11] F. M. Leslie, *Arch. Ration. Mech. Anal.*, Vol. **28**, p. 265 (1968).

[12] S. Onda, T. Miyashita and T. Uchida, *Asia Display*, 33-4 (1998).

[13] H. G. Walton and M. J. Towler, *Liq. Cryst.*, Vol. **27**, p. 1329 (2000)

[14] N. Nagae, T. Miyashita, T.Uchida, Y. Yamada and Y. Ishii, *SID*, p.26 (2000).

[15] H. Nakamura and M. Noguchi, *Jpn. J. Appl. Phys.*, Vol. **39**, P. 6368 (2000).

[16] Y. Zhang, B. Wang, D. B. Chung, J. Colegrove and P. J. Bos, *SID*, 62.5L, p. 1782 (2005).

[17] J. Cheng, R. N. Thurston and D. W. Berreman, *J. Appl. Phys.*, Vol. **52**(4), p. 2756 (1981).

[18] J. Cheng and R. N. Thurston, *J. Appl. Phys.*, Vol. **52**(4), p. 2766 (1981).

[19] S.H. Lee, S.H. Homg, J.D. Noh, H.Y. Kim and D.S. Seo, *Jpn. J. Appl. Phys.*, Vol. **40**, p. L389 (2001).

[20] I. Inoue, T. Miyashita, T. Uchida, Y. Yamada and Y. Ishii, *EuroDisplay*, p. 10-2 (2002).

[21] T. Satake and T. Kurata, *ASID Dig.*, p. 12-6 (2004)

[22] T. Uchida, Y. Kimura, S. Kuniaki, H. Nakamura and Y. Taira, patent JP 9 185 037 (1995)

[23] C. Lee, H. Chang, J. Lyu, K. Kim and J. Souk, *SID Dig*., p-93. (2002)

[24] N. Koma, T. Miyashita, K. Yoneda and T. Uchida, *SID*, p. 5.2 (1999)

[25] M. Xu, D.-K. Yang. P. J. Bos, X. Jin, F. W. Harris and S. Z. D. Cheng, *SID*, 11.4L, p. 139 (1998)

[26] X.-D. Mi, M. Xu, D.-K. Yang and P. J. Bos, *SID*, 5.1, p. 24 (1999)

[27] F. s. Yeung, Y. W. Li and H.-S. Kwok, *Appl. Phys. Lett.*, Vol. **88**, p. 041108 (2006)

[28] F. S.-Y. Yeung, F.-C. Xie, H.-S. Kwok, J. Wau, O. Tsui, and P. Sheng, *SID*, 23.2, p.1080 (2005)

[29] F. S.-Y. Yeung and H.-S. Kwok, *Appl. Phys. Lett.*, Vol. **88**, p. 063505 (2006)

[30] S.H. Lee, T.J. Kim, G.D. Lee, T.H. Yoon, J.C. Kim, *Jpn. J. Appl. Phys*., Vol. **42**, p. L1148 (2001).

[31] E. Acosta, B. Henley, D. Kean, M. Tillin, C. Tombling, M. Towler, E. Walton, H. Walton and R. Winlow, *Liq. Cryst*., Vol. **31**, p.1619 (2004)

[32] C.G. Jhun, J. L. Lee, S. H. Kang, S. L. Lee, J. C. Kim, T.-H. Yoon, J. D. Noh, D. H. Suh and J. Y. Lee, *IDW*, LCTp1-5, p. 117 (2004)

[33] H. Kikuchi, H. Yamamoto, H. Sato, M. Kawakita, K. Takizawa and H. Fujikake, *Jpn. J. Appl. Phys*., Vol. **44**, p. 981 (2005)

[34] M. D. Tillin, E. P. Raynes and M. J. Towler, US Patent, US 6222605 (2001)

[35] F. Bruyneel, H. D. Smet, J. Vanfleteren and A. V. Calster, *Opt. Eng.*, Vol. **40**(2), p. 259 (2001)